Research Square

Preprints are preliminary reports that have not undergone peer review.
They should not be considered conclusive, used to inform clinical practice,
or referenced by the media as validated information.

Visible-Light-Driven Degradation of Organic Dyes Using Novel β- Amino-Modified Cu-BTC MOFs: Toward Clean Water Solutions

Nagina Naveed Riaz
University of Education
Ayesha Faraz
University of Education
Khalil Ahmad
Emerson University, Multan
Ejaz Hussain
Islamia University of Bahawalpur
Muhammad Fiaz
Ajou University
Muhammad Mahboob Ahmed
Bahauddin Zakariya University
Muhammad Kashif
Emerson University, Multan
Ahmad Hosseini Bandegharaei
ahoseinib@semnan.ac.ir

Semnan University

Article

Keywords: Novel β-amino acid-based MOFs, NH2-Cu-BTCs, Photocatalysis, Water remediation, Dye degradation

Posted Date: November 11th, 2026

DOI: https://doi.org/10.21203/rs.3.rs-11397323/v1

License: This work is licensed under a Creative Commons Attribution 4.0 International License.
Read Full License

Additional Declarations: No competing interests reported.

Visible-Light-Driven Degradation of Organic Dyes Using Novel β-Amino-Modified Cu-BTC MOFs: Toward Clean Water Solutions

Nagina Naveed Riaz[*a], Ayesha Faraz[a], Khalil Ahmad[*b], Ejaz Hussain[c], Muhammad Fiaz[d], Muhammad Mahboob Ahmad[e], Muhammad Kashif[b], Ahmad Hosseini Bandegharaei[e, f, g]

[a] Department of Chemistry, Division of Science & Technology, University of Education, 54770 Lahore, Vehari Campus, Pakistan

[b] Department of Chemistry, Emerson University, 60000 Multan, Pakistan

[c] Institute of Chemistry, The Islamia University of Bahawalpur, 63100 Bahawalpur, Pakistan

[d] Department of Chemistry, Ajou University, Suwon 16499, South Korea

[e] Institute of Chemical Sciences, Bahauddin Zakariya University, 60800 Multan, Pakistan

[d] Faculty of Chemistry, Semnan University, Semnan, Iran

[e] Scientific Research Centre, Al-Ayen Iraqi University (AUIQ), Nasiriyah, Thi-Qar, 64001, Iraq

[f] Department of Sustainable Engineering, Saveetha School of Engineering, SIMATS, Chennai, Tamil Nadu 602105, India

[*a] naginanaveed@ue.edu.pk, [*b] khalilnoorpur@gmail.com, ahoseinib@semnan.ac.ir.

Abstract:

In this study, the synthesis and characterization of novel β-amino-functionalized Cu-BTC-MOFs and their photocatalytic performance for dye degradation were carried out. The modified MOFs, denoted as MOF@3A3NP, MOF@3A4HP, and MOF@3A4H3MP, correspond to Cu-BTC functionalized with 3-amino-3-(3-nitrophenyl)propanoic acid, 3-amino-3-(4-hydroxyphenyl)propanoic acid, and 3-amino-3-(4-hydroxy-3-methoxyphenyl)propanoic acid, respectively. PXRD analysis confirmed the synthesis of MOFs having a crystalline structure and FTIR spectroscopy revealed the successful grafting of β-amino functional groups onto the Cu-BTC surface, evidenced by additional peaks at 2130–2233 cm^{-1} and 3350 cm^{-1}. The modified Cu-BTC-MOF exhibited a reduced band-gap energy compared to the unmodified Cu-BTC (2.9 eV) which indicated improved light absorption and charge separation. The β-amino-functionalized Cu-BTC-MOFs demonstrated excellent photocatalytic performance, degrading 95%, 98%, and 99% of methyl green, and 85%, 98%, and 99% of methyl orange in 70 minutes upon exposure to visible light using MOF@3A4HP, MOF@3A4H3MP, and MOF@3A3NP, respectively. This improved photocatalytic activity can be ascribed to the morphological modifications, and reduced optical band gap due to amino-functionalized MOFs. These factors highlight the potential of β-amino-

functionalized Cu-BTC-MOFs as promising photocatalysts for the efficient degradation of both cationic and anionic dyes.

Keywords: Novel β-amino acid-based MOFs, NH_2-Cu-BTCs, Photocatalysis, Water remediation, Dye degradation**.**

Environmental Implications:

The β-amino-functionalized Cu-BTC-MOF developed in this study exhibits exceptional photocatalytic performance under visible light, enabling rapid and efficient degradation of both cationic (methyl green) and anionic (methyl orange) dyes. This advancement addresses a critical environmental challenge by offering a sustainable and energy-efficient solution for wastewater treatment. The reduced band-gap, enhanced surface area, and improved charge separation contribute to superior dye removal efficiency. The use of visible light further enhances the eco-friendliness and practicality of this photocatalyst. These findings highlight its potential application in industrial effluent treatment and broader environmental remediation strategies.

Introduction:

Organic dyes are extensively used coloring agents in nearly all industries, including paper, textile, printing, cosmetics, food, and others. The effluents from these industries are frequently pollute water with these dye residues [1]. Large quantities of dye pollutants in industrial effluents accumulate in waste sources, remains in water over time. These dyes have the potential to seriously endanger aquatic life by causing algal blooms and the depletion of dissolved oxygen in addition to the carcinogenic effects on human health even at the lowest concentrations [2, 3]. Therefore, to lessen the detrimental impacts of dyes on the ecosystem, dyes must be removed from these colorful effluents before they are released into the environment [4]. Among various remediation techniques, photocatalysis has emerged as a superior option for removing organic dyes from water [5]. As of right now, photocatalytic reactions and the adsorption process are thought to be the main techniques for cleaning up organic contaminants in contaminated water [6].

While adsorption is widely investigated due to its straightforward design and ease of operation [7], it merely transfers contaminants from the liquid phase to the solid phase, creating secondary pollution that requires further disposal. Instead of completely removing contaminants, the adsorption process only moves them from one phase to another and lowers their concentration [8].

In contrast, photocatalysis offers a comprehensive environmental cleanup solution by completely mineralizing organic contaminants into harmless inorganic compounds (such as CO_2 and H_2O) under light irradiation, without generating secondary sludge [9]. Materials with metal-organic frameworks (MOFs) are commonly utilized in heterogeneous catalysis and adsorption [10]. Depending on how distinct metals are combined with organic linkers, a range of MOFs has been created for diverse applications [11]. MOFs interest is increasing in a variety of applications, including photocatalysis [12], energy storage [13], pollutant removal [14], and sensing [15]. MOFs have characteristics properties like surface area, variable pore size, pore volume, and desired functionality by post synthetic functionalization [16]. However, a significant number of MOFs exhibit inadequate hydrothermal stability [17], impeding their use in aqueous medium also causing secondary pollution in water due to the presence of organic ligands and metal ions [18]. Consider the Cu-MOF, in liquid samples and high humidity circumstances, water molecules attacked the framework. Due to which the structure collapses and breakdown into organic and inorganic substances [19, 20]. It may be possible to expand the range of applications for these MOFs by making them resistant to water [21]. The degree of binding strength in the metal cluster core and linker essentially determines the hydrothermal stability of MOFs [22]. Increased hydrothermal stability and durability of many different MOFs by ligand functionalization has been reported using a variety of techniques. Using hydrophobic ligands [23], introducing a polymeric matrix [24], hybridization with carbon nano tubes [25, 26] and composite formation with graphite oxide [27, 28] to stop water molecules from attacking metal linker was the way that some researchers attempted to increase hydrothermal stability. The hydrothermal stability of Cu-MOF was enhanced by all these techniques, though their synthesis is rather laborious [29].

Thus, post-synthesis modification of produced MOFs may offer an alternate means of getting around the drawback of inadequate hydrothermal stability [30]. It was proved that the amino acid molecules were grafted onto the Cu-BTC structure to improve hydrothermal stability and prevent water molecules from attacking the exposed metal sites [31]. In amino acid functionalization reactions generally α-positioned amino acids are used although it is assured that β-positioned amino acids possess more potential [32]. Amino acids, chiral ligands with higher valence metal ion centers, are used in functionalization of metal organic frameworks due to their non-toxic and environmentally friendly nature [33]. Amino acids also enhance the stability of structure along with the ability to coordinate with metal center due to nitrogen and carboxyl functionalities [34, 35].

Currently, using MOFs as a photocatalyst is a key area of attention. Due to the abundance of metal-containing nodes and organic bridge linkers, MOFs may be easily and conveniently constructed with a customized capacity to absorb light, making them unique platforms for photo-induced pollution removal [36, 37]. Initially, a material with a specific structure consisting of zinc-based units was employed as a photocatalyst for phenol degradation due to its broad wavelength photosensitivity. Later, titanium-based materials exhibited photocatalytic activity, as predicted, and iron-based materials demonstrated visible light harvesting capabilities [38, 39]. Notably, one material achieved an impressive 96.6% removal of tetracycline and 87.1% removal of dye Rhodamine B upon visible light exposure. The choice of organic linkers in these materials is crucial to enhance their visible-light response. The presence of amine groups in organic ligands has been found to significantly improve the material's ability to respond to visible light. Modified materials have demonstrated superior performance in various applications, including CO_2 reduction, Cr(VI) reduction, and azo dye photodegradation, showcasing their potential as effective visible-light-activated photocatalysts [40, 41].

Due to their affordability, ease of recovery, and environmental friendliness, Cu-based MOFs were chosen as potential catalysts in this work. The amino group was added to the MOF as an additional component for functionalization to improve both visible-light-responsive characteristics and hydrothermal stability. To boost sensitivity to visible light, β-amino-functionalized Cu-BTC was synthesized in this work via post-synthetic modification using a series of three specific β-amino acids: 3-amino-3-(3-nitrophenyl)propanoic acid (yielding MOF@3A3NP), 3-amino-3-(4-hydroxyphenyl)propanoic acid (yielding MOF@3A4HP), and 3-amino-3-(4-hydroxy-3-methoxyphenyl)propanoic acid (yielding MOF@3A4H3MP). Powder X-ray diffraction (PXRD), scanning electron microscopy (SEM), Fourier-transform infrared (FT-IR) spectroscopy, and UV-Vis analysis were used to characterize the materials. The photocatalytic degradation of methyl orange (MO) and methyl green (MG) was evaluated under simulated solar light irradiation (visible light) to assess the performance of these β-amino-functionalized Cu-BTC catalysts. This work provides fresh insights into the optimization of β-amino acid-based photocatalysts for the efficient degradation of organic dyes.

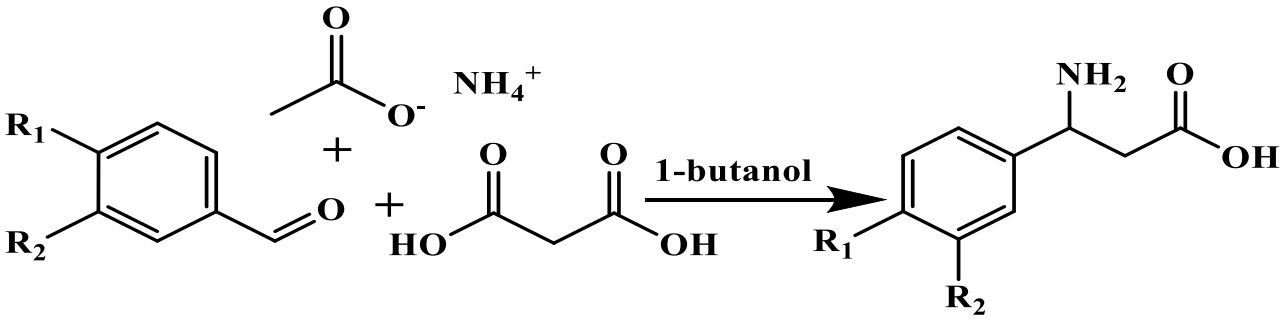
Experimental:

Materials:

Chemicals used for the synthesis of β-amino acids and MOF materials include malonic acid, ammonium acetate, 3-nitro benzaldehyde ($HNO_2C_6H_4CHO$;99%), 4-hydroxy benzaldehyde (HOC_6H_4CHO;99%), 4-hydroxy-3-methoxy benzaldehyde ($HOC_6H_3(OCH_3)CHO$;99%), 1-butanol were purchased from Merck Company (Germany)., copper (II)nitrate trihydrate, 1,3,5-benzenetricarboxylic acid (H_3BTC, 99%; Sigma Aldrich), deionized water, ethanol, acetone and methanol.

Synthesis of β-amino acid:

To synthesize β-amino acid, respective aldehydes, malonic acid, and ammonium acetate in equimolar ratios (10 mmol) with 1-butanol as solvent (50 mL). The mixture was heated to reflux and stirred for 3 hours (Scheme 1). Following this, the resulting product was recovered by filtration, washed with acetone to remove impurities, and then dried in a controlled temperature oven at 150°C for 12 hours to remove any residual solvents [42]. For 3-Amino-3-(3-nitrophenyl) propanoic acid (3A3NP), melting point; 186 ºC, for 3-Amino-3-(4-hydroxyphenyl) propanoic acid (3A4HP), melting point, 189 ºC and for 3-Amino-3-(4-hydroxy-3-methoxyphenyl) propanoic acid (3A4H3MP), melting point; 192 ºC was measured.



Scheme 1. Synthesis of β-amino acid. For synthesis aldehydes having R1 and R2 different groups given in Table 1.

Table.1 Numbering of substituents for the synthesis of β-amino acids.

β-amino acid	R_1	R_2
3A3NP	H	NO_2
3A4HP	OH	H
3A4H3MP	OH	OCH_3

Synthesis of Cu-BTC MOF:

Initially, 2.2g of $Cu(NO_3)_2.3H_2O$ was dissolved in 20ml of deionized water to form a solution, while 1.2g of benzene tricarboxylic acid was separately dissolved in 20 mL of deionized water. The two solutions were then combined and transferred to a 100 mL Teflon-lined stainless-steel autoclave reactor. The mixture was subsequently subjected to microwave radiation at 220 °C for 8 hours in an oven, resulting in the formation of the desired product. After cooling, the product was recovered by filtration, washed extensively with ethanol, and dried. The product was then suspended in methanol for 52 hours to facilitate activation for further functionalization. Finally, the Cu-BTC MOF was dried at 90 °C for 24 hours to remove any residual solvents [43, 44].

Synthesis of Novel Cu-BTC@β-amino acid Composite:

The functionalization of copper metal-organic framework (Cu-BTC) with β-amino acids was achieved by adding the β-amino acid in an amount equivalent to 30% of the weight of copper in the Cu-BTC MOF. Initially, the β-amino acid(3-Amino-3-(3-nitrophenyl) propanoic acid, 3-Amino-3-(4-hydroxyphenyl) propanoic acid, 3-Amino-3-(4-hydroxy-3-methoxyphenyl) propanoic acid) was dissolved in 50 mL of deionized water and stirred for 1 hour at 50 °C. Subsequently, the Cu-BTC MOF was added to the solution, and the reaction was set to proceed for 24 hours at 55 °C. The resulting product was recovered by filtration, washed with acetone to remove impurities [43, 44]. The multiple stages of the synthesis process of the Cu-BTC@ β-amino acid Composite are illustrated in **Scheme 2**. These final functionalized materials are hereafter referred to as Cu-BTC@3A3NP, Cu-BTC@3A4HP, and Cu-BTC@3A4H3MP, respectively, corresponding to the specific β-amino acid used for the modification.

Photocatalytic studies:

In order to study the photocatalytic activity of the β-amino acid-functionalized metal-organic frameworks, 50 mg of the catalyst was added to 100 mL of a 10 ppm solution of methyl green and methyl orange dyes. (Note: While raw industrial textile wastewater may exhibit higher dye concentrations, 10 ppm represents a realistic concentration for secondary-treated effluents and serves as a standard model concentration to evaluate fundamental photocatalytic mechanisms and catalyst efficiency prior to scale-up). To assure the dye adsorption/desorption phenomenon, the reaction flask was covered with aluminum foil and stirred at 250 rpm for 30 minutes in the dark. Following this, the reaction flask was placed under a visible light source e.g., a 300 W Xenon arc lamp equipped with a UV cutoff filter ($\lambda > 420$ nm) to simulate solar irradiation. Small portions of the suspension were withdrawn at regular time intervals (every 10 minutes), and the absorbance was measured using a UV-Vis spectrophotometer. To obtain the maximum degradation, three key operational parameters were systematically optimized and studied: catalyst dosage (10–75 mg), solution pH (3–12), and contact time (0–90 minutes).

Under visible light irradiation, degradation of methyl orange and methyl green was explored so as to evaluate the photocatalytic performance of amino acid functionalized metal organic frameworks. The solutions containing samples were first stirred in dark for 30 minutes to let the dyes and photocatalyst to attain adsorption/desorption equilibrium. Following visible light irradiation 8 samples of each dye were taken after regular interval of 10 minutes and the absorbance was measured. Under solar light irradiation it was found that Cu-BTC MOF showed degradation of methyl green and methyl orange dyes. It was demonstrated that β-amino acid modified MOFs (Cu-BTC@3A3NP, Cu-BTC@3A4HP, Cu-BTC@3A4H3MP) showed more potential effects towards the degradation of dyes. After regular intervals the absorbance spectra showed that the absorbance was decreased. The percentage value for photocatalytic degradation of dyes was also calculated by using the formula:

$$\% \text{ degradation} = \frac{Ao - At}{Ao} X\ 100 \quad (1)$$

A_o = initial absorbance, A_t = absorbance at regular time interval

All the three parameters (amount of catalyst, pH of dye solution and contact time) to obtain the maximum degradation of dyes were optimized and effects were studied by obtaining their UV-vis spectra.

For the binary dye experiments, a mixed solution was prepared by combining appropriate volumes of methyl orange and methyl green stock solutions to yield a final reaction volume of 100 mL containing 10 ppm of each dye simultaneously.



Scheme 2. A systematic procedure for the synthesis of Cu-BTC@β-amino acid Composite.

Characterization of synthesized MOFs:

The structural characteristics of the synthesized samples were examined using a PXRD and the instrument was configured to utilize Cu Kα radiation with a wavelength of 1.540 Å, and the scan speed was set at 2° per second. The 2θ range was established as 10-70°, allowing for a comprehensive analysis of the samples' structural properties. The surface morphology of the synthesized samples was examined using a SEM instrument in the range of 5 micro-meter, which provided detailed information about their structural features. Furthermore, a FTIR spectrometer was employed to investigate the presence of functional groups in the samples with Bruker FTIR

Spectrophotometer (ZnSe) TENSOR27 (USA). The FTIR spectrum was generated with a resolution of 4 cm^{-1}, and the transmission wavelength range was set at 4000-400 cm^{-1}, enabling the detection of a wide range of functional groups. ^{1}H and ^{13}C NMR spectra's of β-amino acids were also calculated with the help of Bruker AM 400 NMR spectrometer (USA). Additionally, the optical properties of as synthesized samples were studied by acquiring UV-visible absorbance spectra using a CEISEL 7000 UV-visible spectrophotometer, which allowed for the analysis of their light-absorbing characteristics.

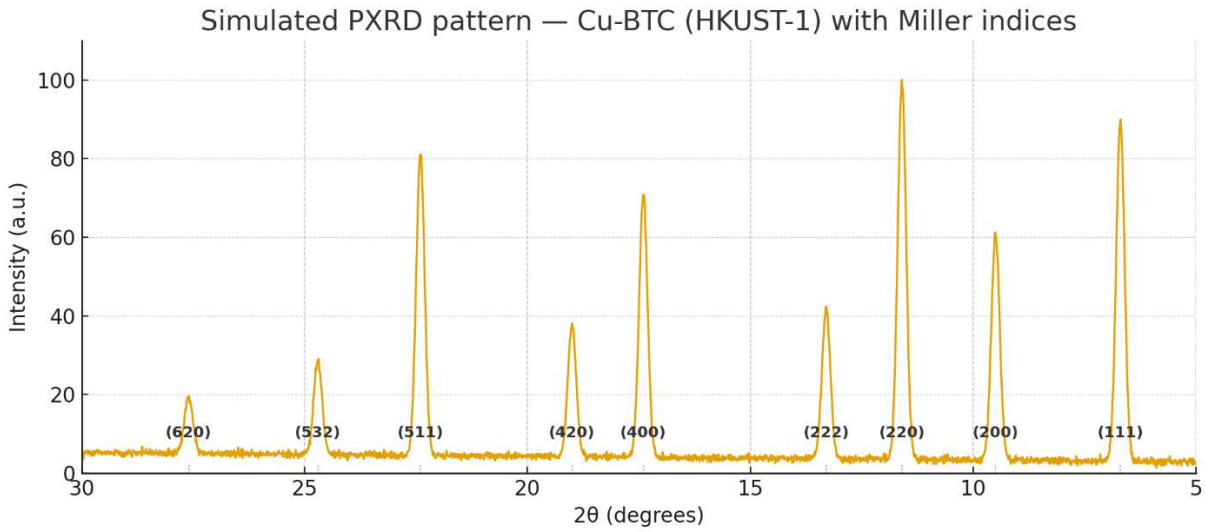
Results and discussion:

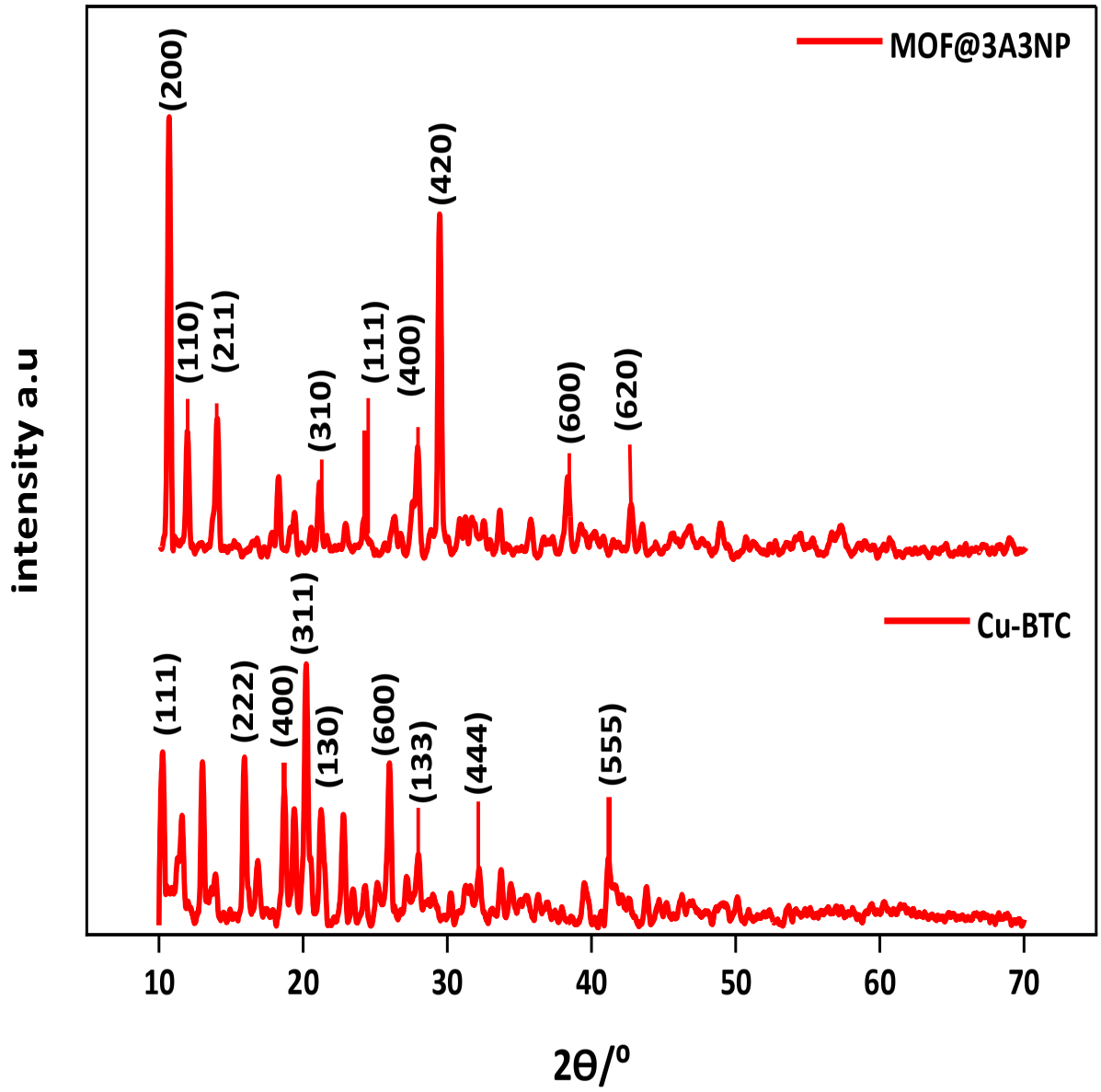
PXRD analysis:

The peak positions of the prepared Cu-BTC MOF and Cu-BTC@3A3NP, Cu-BTC@3A4HP, and Cu-BTC@3A4H3MP all exhibit a cubic crystal structure similar to the reported patterns and are consistent with the literature [45-47]. Minor discrepancies in peak intensity and slight shifts between the simulated and experimental PXRD patterns of pristine Cu-BTC MOF are commonly observed in solvothermally synthesized MOFs. These variations are typically attributed to the presence of trapped guest solvent molecules within the pores, preferred orientation of crystallites during sample preparation, or minor surface defects. Nevertheless, the strong peak at 10.28° corresponds to the (111) reflection, which is a characteristic peak for Cu-BTC MOF, confirming that the fundamental crystal structure is retained. The other peaks indexed to the (200), (220), (400), (600), (420) reflections are also consistent to the cubic crystal and showed an average lattice parameter of 24.4Å. The peak positions and corresponding crystal planes in patterns of β-amino acid modified MOFs are also comparable to the parent MOF. This indicating that crystal structure is retained, and amino acid is only coordinated with the copper metal atom[43] (**Figure 1**). The average lattice parameter calculated for Cu-BTC@3A3NP, Cu-BTC@3A4HP, Cu-BTC@3A4H3MP also gave approximately 24.4Å value with an additional peak at 24.3º, 25.9º and 24,02º. These peaks are assigned to β-amino acid in Cu-BTC@3A3NP, Cu-BTC@3A4HP, Cu-BTC@3A4H3MP respectively which is not present in Cu-BTC MOF. The enhanced intensity and slight shifting of peak at 29º from 28.1º is also attributed to the amino acid incorporation in these structures. Distance between the planes of the crystals (d) was calculated and all the parameters and crystal planes suggested

a Fm-3m face centred cubic structure for the prepared MOFs having a=b=c with angles α=β=ɤ=90º [48, 49]. All the lattice parameters were determined according to the Bragg's law equation:

$$2d\sin\Theta = n\lambda \qquad (2)$$




MOF@3A3NP
(200)
(110)
(211)
(310)
(111)
(400)
(420)
(600)
(620)
Cu-BTC
(111)
(222)
(400)
(311)
(130)
(600)
(133)
(444)
(555)
intensity a.u
10
20
30
40
50
60
70
2Θ/º

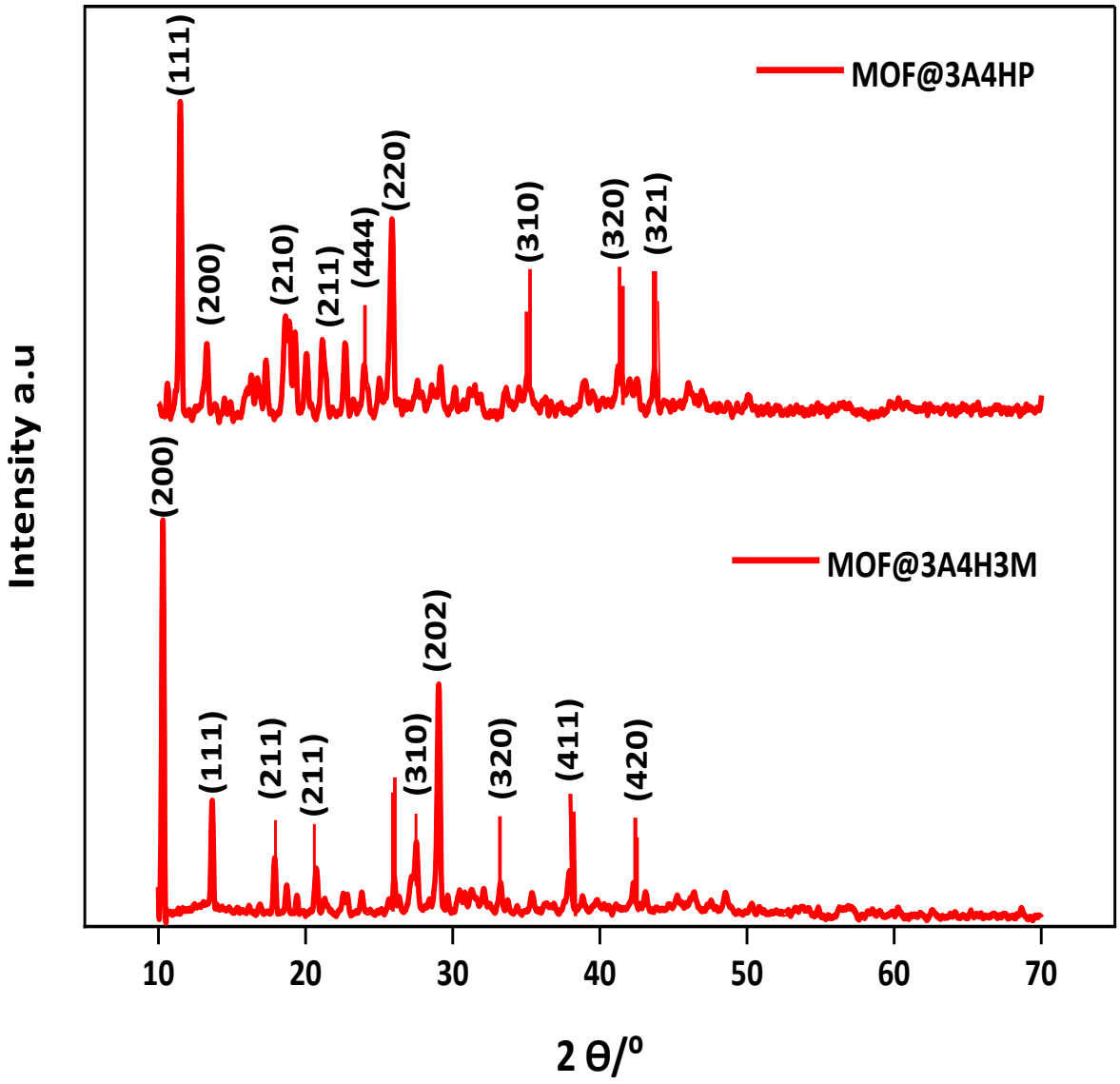


Figure 1. Simulated PXRD patterns of Cu-BTC, PXRD of Cu-BTC and β-amino acids modified MOFs.

SEM analysis:

The SEM images reveal a striking difference in the surface morphology of Cu-BTC MOF before and after amino acid modification. Prior to modification, the Cu-BTC MOF crystals exhibit large, well-defined cubic shapes with visible pores and active sites. In contrast, the modified Cu-BTC composites displays a significantly altered surface topology, characterized by a feather-like appearance and a reduction in apparent particle size compared to the unmodified Cu-BTC MOF

(**Figure 2**). This reduction in particle size and morphological change can be attributed to the post-synthetic coordination of bulky β-amino acid molecules to the open metal sites on the surface of the Cu-BTC MOF crystals. This surface functionalization introduces steric hindrance, disrupts the long-range crystalline order at the crystal periphery, and induces slight surface restructuring, thereby preventing further crystal growth and yielding smaller, more compact particles. This transformation suggests that the amino acid functional groups have effectively grafted onto the Cu-BTC MOF surface, modifying its morphology and potentially enhancing its photocatalytic properties by improving reactant adsorption and charge carrier mobility.

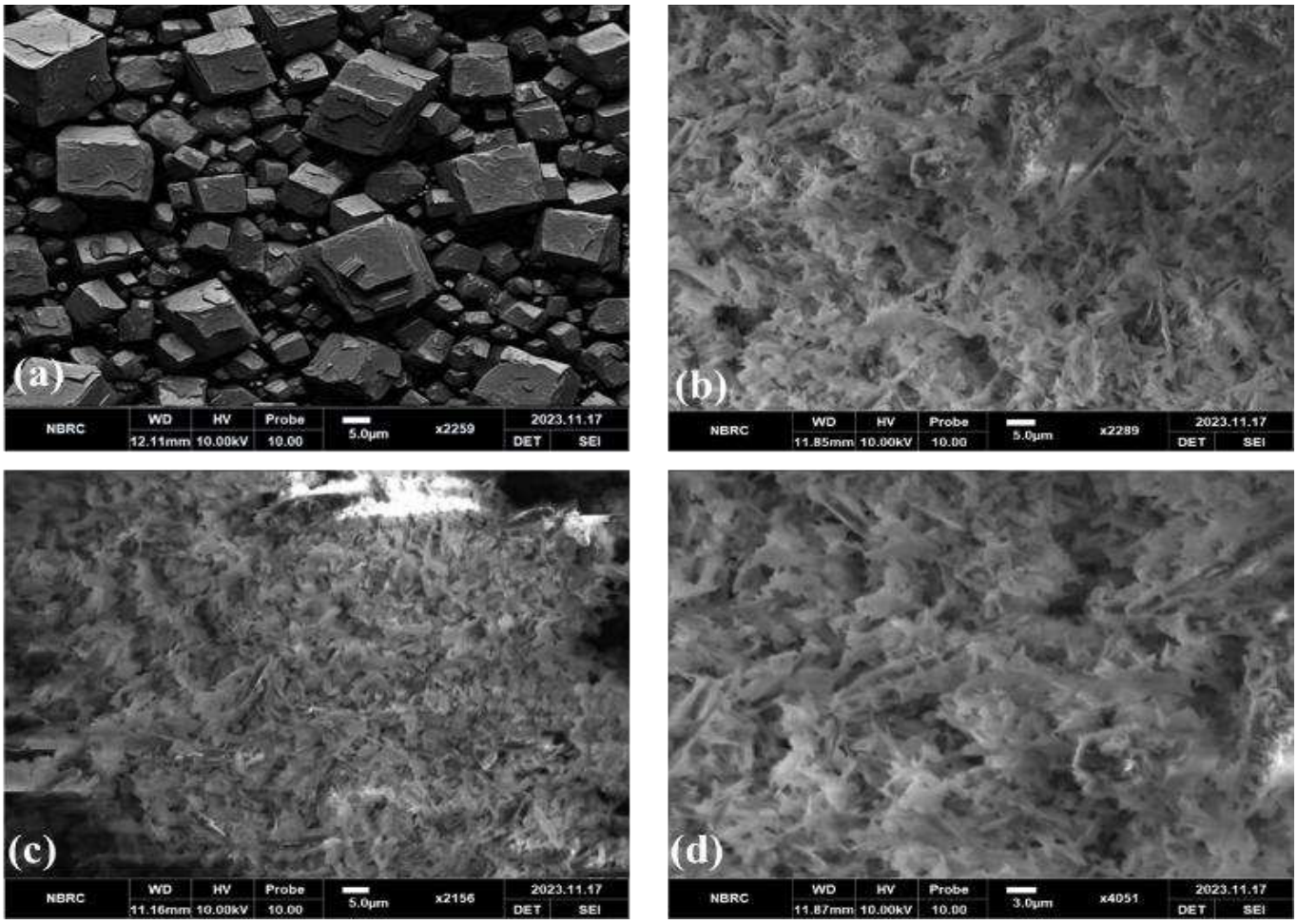


Figure 2. SEM images of the synthesized Cu-BTC MOF and their composites, showing the morphological changes upon functionalization. (a) SEM images of Cu-BTC MOF at 5 μm magnification, e.g., 2250× magnification, (b) Cu-BTC@3A3NP Cu-BTC MOF at 5 μm magnification, e.g., 2250× magnification, (c) Cu-BTC@3A4HP Cu-BTC MOF at 5 μm

magnification, e.g., 2156× magnification , (d) Cu-BTC@3A4H3MP Cu-BTC MOF at 3 μm magnification, e.g., 4051× magnification.

FTIR analysis:

FTIR analysis of the prepared materials was performed to verify the functional groups and confirm the successful incorporation of the β-amino acids onto the Cu-BTC MOF framework. In the pristine Cu-BTC MOF spectrum, the peak at ~697 cm^{-1} is associated with the metal-ligand Cu–O bond, while the peak at 1193 cm^{-1} corresponds to the C–O stretching vibrations of the BTC linker. The peak at 1444 cm^{-1} indicates the bending vibrations of CH_2, and the peak at 1569 cm^{-1} is assigned to the aromatic C=C stretching vibration. Additionally, peaks in the region of 1632 cm^{-1} and 1711 cm^{-1} correspond to the symmetric and asymmetric stretching vibrations of the carbonyl group, respectively. A broad band at ~3404 cm^{-1} indicates the presence of hydrated OH groups in the parent MO [43, 44, 50]. Upon functionalization, the spectra of the modified MOFs (Cu-BTC@3A3NP, Cu-BTC@3A4HP, and Cu-BTC@3A4H3MP) retain all the characteristic peaks of the parent Cu-BTC, confirming that the fundamental framework structure is preserved. Crucially, new peaks emerge that validate the successful grafting of the β-amino acids. Specifically, the peaks in the range of 2850–2950 cm^{-1} are now correctly assigned to the aliphatic and aromatic C–H stretching vibrations of the amino acid backbone. The successful coordination is further evidenced by the appearance of a distinct C–N stretching vibration in the region of 1200–1250 cm^{-1}, which is absent in the pristine Cu-BTC MOF. Furthermore, the N–H stretching vibrations of the primary amine groups are clearly resolved in the 3300–3400 cm^{-1} region (overlapping with the broad O–H stretch). The presence of these specific C–H, C–N, and N–H vibrational modes, alongside the preserved Cu–O and BTC linker peaks, provides strong spectroscopic evidence that the β-amino acids have been successfully anchored to the open metal sites of the Cu-BTC MOF framework via post-synthetic modification [42, 51] (**Figure 3**).

Upon functionalization, the spectra of the modified MOFs retain the characteristic peaks of the parent Cu-BTC MOF, confirming that the fundamental framework structure is preserved. Additionally, new vibrational modes emerge in the spectra, including broadened bands in the 3300–3400 cm^{-1} region (overlapping N–H and O–H stretches) and new features in the fingerprint region, which are suggestive of the incorporation of the β-amino acid moieties. We acknowledge, however, that while FTIR provides strong corroborative evidence of modification, it cannot

definitively distinguish between strong surface physisorption and true coordination grafting on its own, nor does it quantify the exact loading of the amino acid. The successful functionalization is therefore inferred from the combination of these FTIR changes, the retention of crystallinity observed in PXRD, and the distinct changes in photocatalytic behavior.

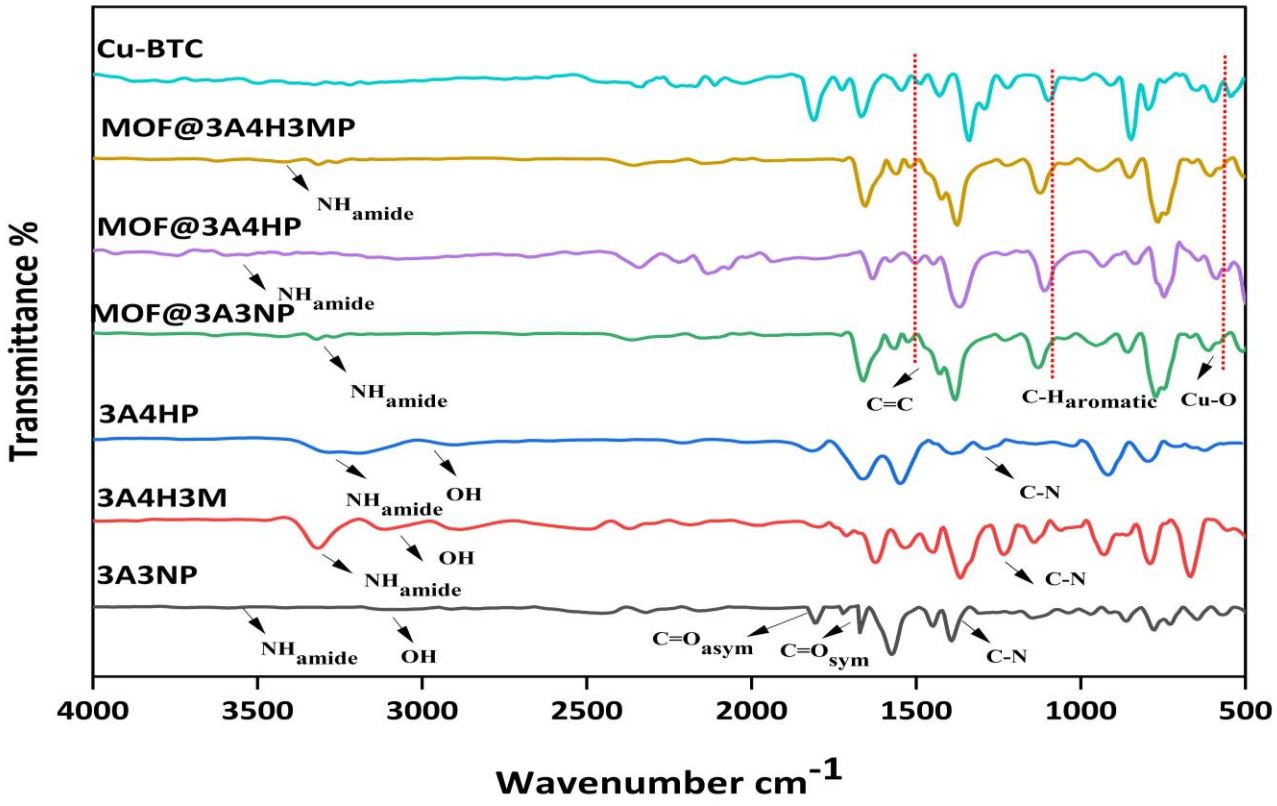


Figure 3. FTIR Spectra of β-amino acids, Cu-BTC MOF and β-amino acid modified Cu-BTC composites.

^{1}H NMR analysis:

The ^{1}H NMR spectra of three amino acids, 3-amino-3-(4-hydroxyphenyl)propanoic acid, 3-amino-3-(4-hydroxy-3-methoxyphenyl)propanoic acid, and 3-amino-3-(3-nitrophenyl)propanoic acid, confirm their structures. The spectra exhibit characteristic resonances for aliphatic protons (2.13-4.7 ppm), aromatic protons (6.9-7.7 ppm and 7.01-7.5 ppm), and hydroxyl protons (10.11 ppm). Specifically, 3-amino-3-(4-hydroxyphenyl)propanoic acid shows resonances at 2.63-2.88 ppm for aliphatic and 4.28-4.40 ppm also for aliphatic and 7.16 to 8.54 ppm for aromatic protons. 3-amino-3-(4-

hydroxy-3-methoxyphenyl)propanoic acid at 2.90-4.36 ppm for aliphatic and 6.81-7.79 ppm for aromatic, and 3-amino-3-(3-nitrophenyl)propanoic acid at 2.64-2.90 ppm, 4.18-4.58 ppm for aliphatic, and 7.5 to 8.18 ppm for aromatic protons[42, 52] (**Figure S1-S6**). These findings are consistent with the ^{13}C NMR results, which revealed distinct carbon resonances for the aliphatic backbones, aromatic rings, and functional groups (hydroxy, methoxy, and nitro), confirming the proposed structures.

^{13}C NMR analysis:

The ^{13}C NMR spectroscopic analysis of the three compounds provided valuable insights into their molecular structures. The spectrum of 3-amino-3-(4-hydroxyphenyl)propanoic acid exhibited resonances at 42.94, 53.15, 115.5, 128.2, 137.54, 173.21 ppm. This confirms the presence of an aromatic ring, a propanoic acid backbone, and a carboxylic acid group. In contrast, the 3-amino-3-(4-hydroxy-3-methoxyphenyl) propanoic acid spectrum displayed additional resonances at 114.16, 115.23, 122.26, 123.31, 124.63, and 194.55 ppm. This indicate the methoxy group and an ester or amide carbonyl. The 3-amino-3-(3-nitrophenyl)propanoic acid spectrum showed resonances at 43.41, 43.63, 43.73, 43.92, 44.12, and 177.34 ppm, due to propanoic acid backbone, a nitrophenyl group, and a carboxylic acid group [42, 52] (**Figure S1-S6**). These findings demonstrate the utility of ^{13}C NMR spectroscopy in elucidating the structural differences among these compounds, highlighting the impact of substituents on the aromatic ring.

Optical properties

UV-vis absorption spectra are shown in **Figure 4** for the prepared MOF, before and after modification with β-amino acid. The spectrum of Cu-BTC MOF exhibits a peak at 250-300 nm, referred to π- $\pi*$ transitions in the aromatic rings in the BTC ligand and charge transfer transitions between the Cu (II) ions and the BTC ligand. A weak absorption region at 500 nm is also observed, corresponding to d-orbital transitions of the Cu (II) ions [1, 53]. In contrast, the spectrum of amino acid functionalized Cu-BTCs show additional peaks in the range of 350 nm. These peaks are attributed to the absorption of the amino acid functional groups. This peak suggests the formation of a pi-complex between the amino acid and the Cu (II) ions, indicating successful functionalization. The weak absorption at 500 nm is similar to that observed in Cu-BTC, corresponding to d-d transitions of the Cu (II) ions and ligand field transitions involving the Cu (II) ions and the BTC ligand [54-56]. Amino acid

functionalization leads to a bathochromic shift (red shift) in the UV-Vis spectrum suggests that the amino acid functionalization has successfully introduced new electronic transitions, leading to improved optical and electronic properties. Band gap energy value for both the Cu-BTC MOF and β-amino acid modified composite was determined from UV-Vis spectrum according to the Tauc plot by following the equation:

$$(\alpha h\nu) = A\,(h\nu - Eg)^{m} \qquad (3)$$

α is the absorption coefficient, hν is the photon energy, A is a constant, Eg is the band gap energy, m is an exponent that depends on the transition type: m = 1/2 for indirect allowed transitions. m = 2 for direct allowed transitions, m = 3/2 for indirect forbidden transitions, n = 3 for direct forbidden transition. Extrapolating the linear region gave the band gap energy value. Cu-BTC MOF has a larger band gap energy 2.9 eV, indicating a wider energy gap between the valence and conduction bands. This suggests that the material has a higher energy barrier for electrons to transition from the valence to conduction band. Cu-BTC@3A3NP has a band gap energy 2.2 eV, Cu-BTC@3A4HP 1.84 eV and Cu-BTC@3A4H3MP 2.75 eV indicating a narrower energy gap between the valence and conduction bands and band gap of other materials are given in (**Figure S7-S10**). This suggests that the amino acid modification has reduced the energy barrier for electrons to excitation from the valence level to conduction level, making it easier for electrons to flow, which is a promising sign for enhanced photocatalytic activity.

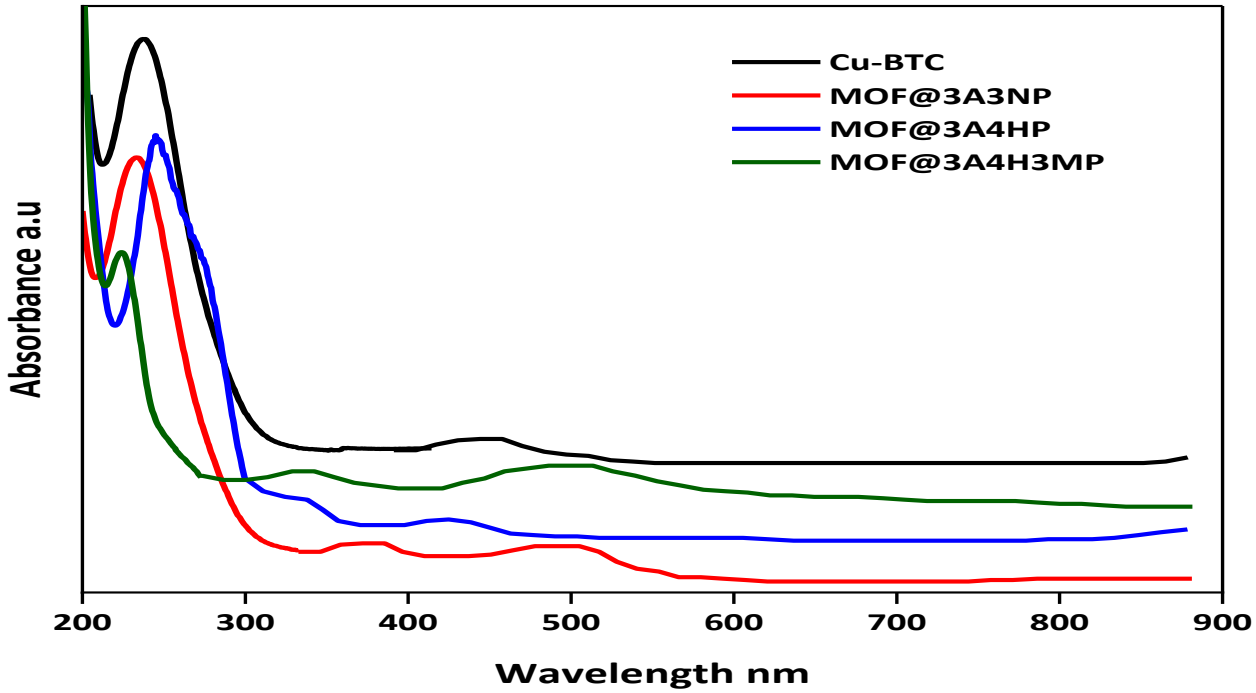


Figure 4. UV-Vis spectra of Cu-BTC MOF and β-amino acid modified Cu-BTC composites.

Point of Zero charge:

The point of zero charge is a crucial parameter in determining the net surface charge of a photocatalyst in an aqueous solution. It reveals that the pH at which the surface charge shifting occurs. The pH drift method, a previously described method was used to determine the PZC [43]. The PZC was determined by measuring the final pH of 8 samples with varying initial pH from 3 to 10, after 48 hours of equilibrating in 0.01M NaCl solution. The material's point of zero charge is 7.7 for Cu-BTC@3A3NP, 7.9 for Cu-BTC@3A4HP and 7.8 for Cu-BTC@3A4H3MP (**Figure S11-S13**).

Photocatalytic properties

Effect of amount of photocatalyst

The effect of catalyst amount on dye degradation was investigated, revealing a significant enhancement in degradation efficiency with increasing catalyst loading up to a threshold. Specifically, 10mg of catalyst, 24.5%, 15% and 24.5% of the dye was degraded within 50 minutes. 25mg of catalyst, 51%, 47% and 50% of the dye was degraded within 50 minutes. 50mg of catalyst, 86.9%, 69.2% and 82.4% of the dye was degraded within 50 minutes. 75mg of catalyst, 86%, 68.3% and 81.3%of the dye was degraded within 50

minutes (a slight decrease) for methyl green with Cu-BTC@3A3NP, Cu-BTC@3A4HP, Cu-BTC@3A4H3MP respectively. Similarly, 10mg of catalyst, 21%, 18% and 18% of the dye was degraded within 50 minutes. 25mg of catalyst, 46%, 21% and 39% of the dye was degraded within 50 minutes. 50mg of catalyst, 52%, 46%, 48% of the dye was degraded within 50 minutes. 75mg of catalyst, 50%, 45% and 47% of the dye was degraded within 50 minutes with Cu-BTC@3A3NP, Cu-BTC@3A4HP, Cu-BTC@3A4H3MP respectively (**Figure S14**).

This indicates that the catalyst amount has a profound impact on the degradation efficiency, with higher amounts leading to faster and more extensive dye degradation up to an optimal point (50mg). Beyond this point, further increases in catalyst amount (75mg) do not lead to additional degradation, and even result in a slight decrease, suggesting a possible inhibition effect or saturation of active sites [1].

(Ensure this sentence remains to fix the time alignment)

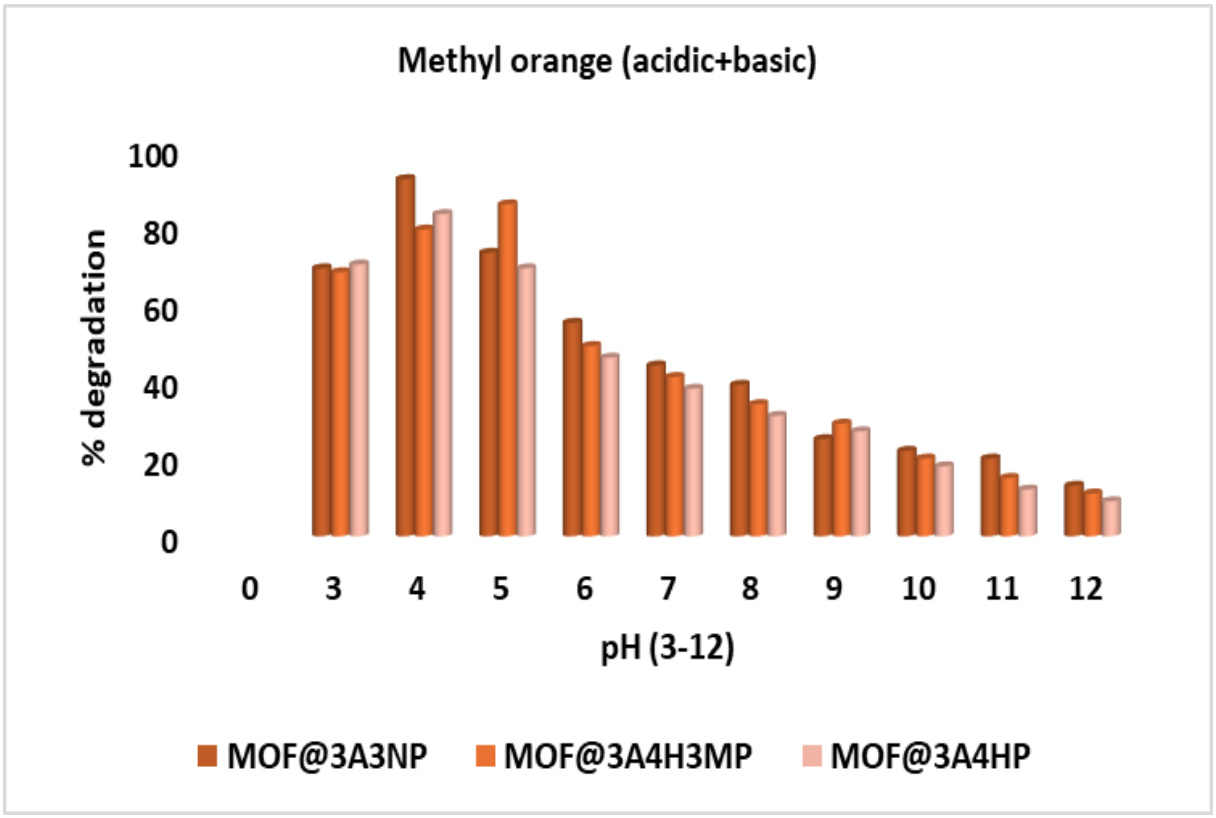
"To assure the dye adsorption/desorption phenomenon, the reaction flask was covered with aluminium foil and stirred at 250 rpm for 30 minutes in the absence of visible light (represented as -30 to 0 minutes in the kinetic graphs). Following this dark equilibrium period, the flask was placed under a visible light source

Effect of acidity and basicity of dye solution

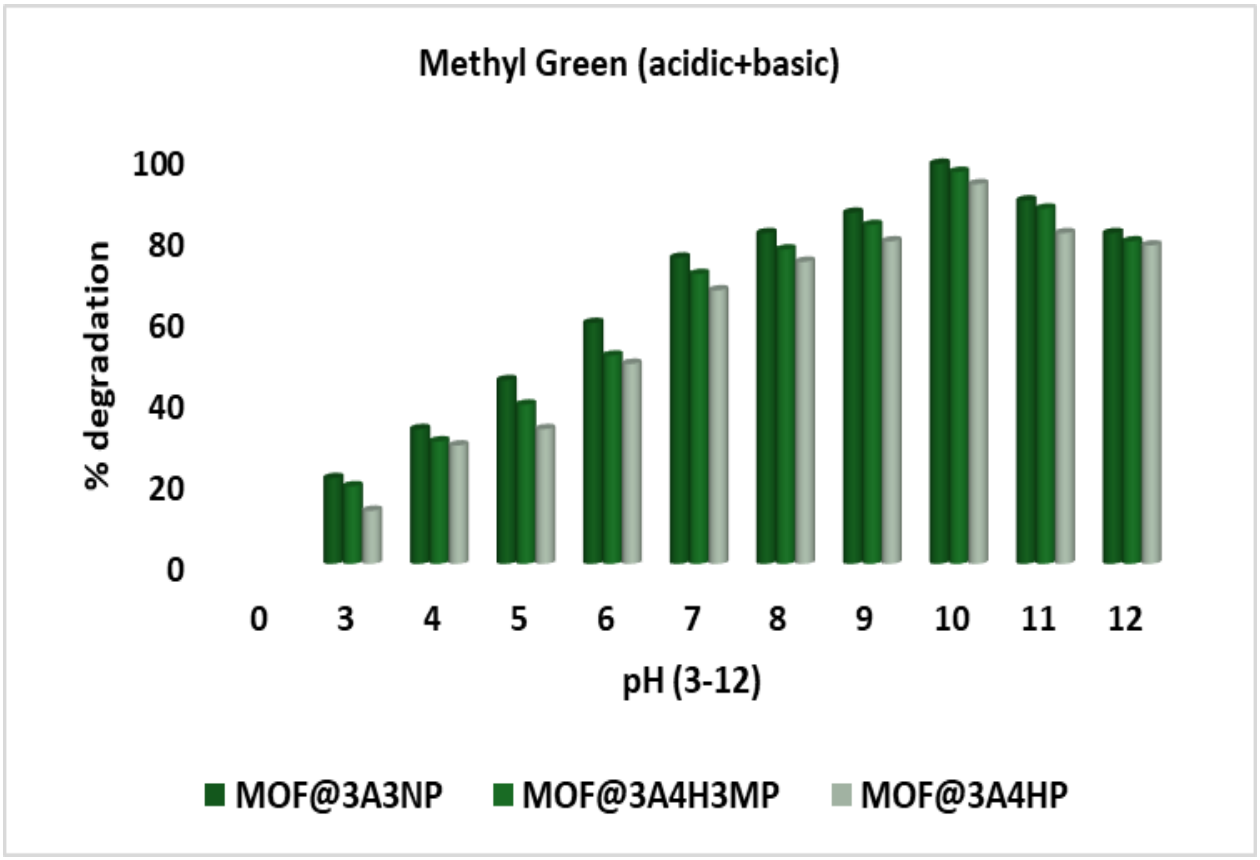
The value of pH is an important factor which effect the photocatalytic degradation of dye due to the presence of surface charge.[36] Varied pH levels resulted in the different active species present in the system for photocatalysis. The positively charged holes and electron pairs served as primary catalytic species [57]. The amino group in the MOFs acts as electron donor and decrease the recombination in acidic condition resulting in increased degradation due to the presence of holes [36]. While in basic conditions -OH combine with the holes and produce radicals with higher ability to cause degradation [58].

Further studies to investigate the effect of pH on degradation of dyes experiment was conducted in acidic and basic conditions for both the dyes. For acidic conditions pH from 3 to 7 was selected. Similarly, for basic conditions pH was adjusted between 8 to 12 for both the dyes. It was observed that MOFs showed maximum degradation of methyl orange in acidic pH=4 for Cu-BTC@3A3N and Cu-BTC@3A4HP while for Cu-BTC@3A4H3MP pH=5 with 92%, 83% and

85.5% degradation respectively. Similarly, maximum degradation of methyl green in basic pH=10 with 98%, 96% and 93% photocatalytic degradation of dye in 50 minutes by using Cu-BTC@3A3NP, Cu-BTC@3A4HP, Cu-BTC@3A4H3MP (**Figure S15**). At lower pH positive charge from amino group wins making the surface slightly positive. At higher pH the negative charge from the nitro group wins making the surface charge slightly negative. This dynamic surface charge created by the modification, allows the material to adapt to changes in pH and degrade both cationic and anionic dyes (**Figure 5**). In acidic conditions, the protonation of MO enhances electrostatic attraction with the negatively charged MOF surface, facilitating degradation. Conversely, MG is cationic and exhibits stronger interaction with the MOF in basic medium due to deprotonation of surface groups, improving adsorption and degradation efficiency.


Methyl orange (acidic+basic)
% degradation
100
80
60
40
20
0
0
3
4
5
6
7
8
9
10
11
12
pH (3-12)
MOF@3A3NP
MOF@3A4H3MP
MOF@3A4HP

419


Methyl Green (acidic+basic)
% degradation
100
80
60
40
20
0
0
3
4
5
6
7
8
9
10
11
12
pH (3-12)
MOF@3A3NP
MOF@3A4H3MP
MOF@3A4HP

420

Figure 5. Graphs showing effect of acidity and basicity of dye solution on percentage degradation of two dyes methyl orange and methyl green.

Effect of contact time

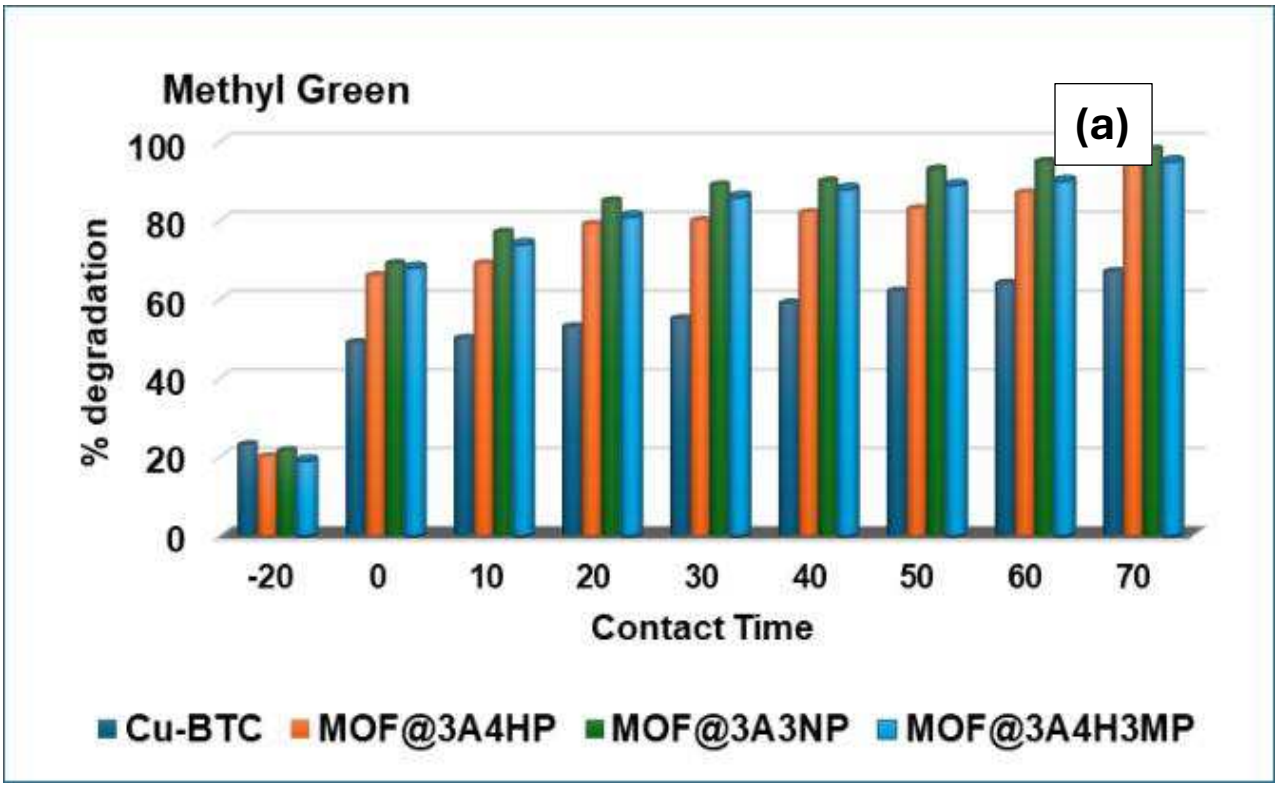
As modified MOFs has demonstrated exceptional photocatalytic activity, achieving maximum degradation of methyl green and methyl orange dyes within 70 minutes. This highlights its potential as a highly effective photocatalyst for dye degradation. The incorporation of specific amino groups (3A3NP, 3A4HP, 3A4H3MP) into the MOF structure has significantly enhanced its photocatalytic efficiency. The optimized band gap of the prepared MOF enables efficient harnessing of visible light, reducing the recombination of photo-generated electron-hole pairs and thereby boosting its photocatalytic performance. In photocatalytic process, the presence of amino groups in MOFs enhances the catalyst's electron transfer capabilities, leading to improved oxidation potential and increased degradation of dye molecules [39]. Prolonged solar irradiation and the use of Cu-BTCNH_2 as a catalyst also facilitate the removal of dyes [59]. The photocatalytic process involves the generation of positively charged holes by organic ligands. This transfer of photo-initiated electrons to metal nodes, resulting in a charge transfer process that drives the degradation of dyes through oxidation. The amino groups in the metal-organic frameworks can reduce the reunion of electrons and holes, prolonging the oxidation and degradation process [60-62] (**Figure 6 a & b**).

Prior to exposure to sunlight, the dye solutions containing the samples were allowed to reach adsorption-desorption equilibrium by being kept in the dark for 30 minutes. Then, the solutions were stirred under sunlight, and samples were collected at 10-minute intervals to assess the photocatalytic degradation of the dyes. This procedure enabled the evaluation for all the four samples' photocatalytic activity under sunlight irradiation.

Cu-MOFs struggled to remove dyes through direct adsorption in the absence of light. However, when exposed to sunlight, Cu-BTC-NH_2 exhibited enhanced catalytic properties, leading to significantly improved dye removal. The degree of improvement was directly proportional to the duration of irradiation, with optimal degradation achieved at 70 minutes upto 99.1% degradation. Thus, this comparison showed that modified MOFs gave better results than the parent MOF. The recyclability of the synthesized MOFs was tested over five consecutive

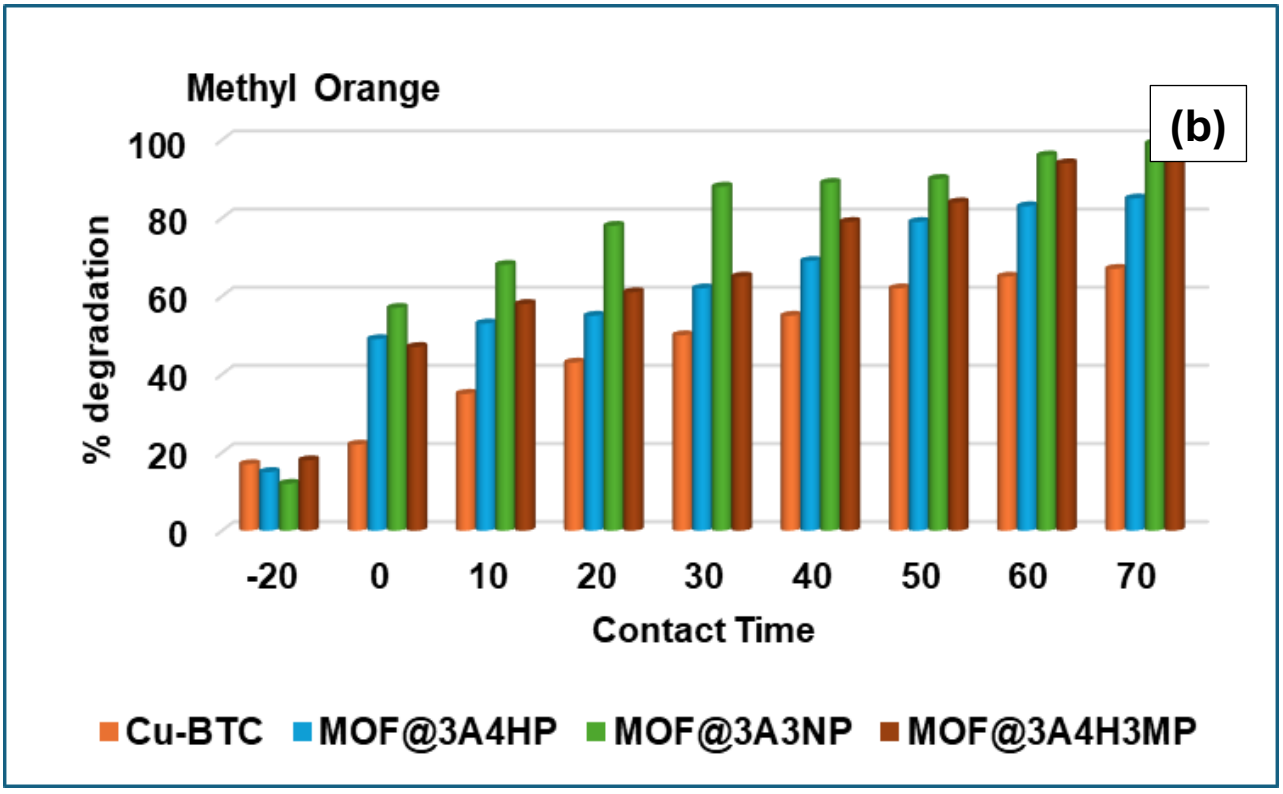
photocatalytic cycles. The MOFs retained more than 85% of their initial degradation efficiency after five cycles, demonstrating good stability and reusability under the experimental conditions.

The recyclability of the synthesized MOFs was tested over five consecutive photocatalytic cycles. The MOFs retained more than 85% of their initial degradation efficiency after five cycles. While direct hydrothermal stability tests (such as prolonged water-soaking followed by PXRD) were not performed in this study due to instrumental constraints, this consistent performance over multiple cycles in aqueous media serves as strong indirect evidence of the framework's structural integrity and resistance to rapid degradation under operational photocatalytic conditions.


Methyl Green
(a)
100
80
60
40
20
0
% degradation
-20
0
10
20
30
40
50
60
70
Contact Time
Cu-BTC
MOF@3A4HP
MOF@3A3NP
MOF@3A4H3MP

458

459


Methyl Orange
(b)
100
80
60
40
20
0
% degradation
-20
0
10
20
30
40
50
60
70
Contact Time
Cu-BTC
MOF@3A4HP
MOF@3A3NP
MOF@3A4H3MP

460

Figure 6. Graphs representing the degradation of (a) methyl orange and (b) methyl green by amino acid modified MOFs (Cu-BTC@3A3NP, Cu-BTC@3A4HP, Cu-BTC@3A4H3MP) with contact time and their % degradation efficiencies. The x-axis explicitly denotes the dark adsorption equilibrium phase from -30 to 0 minutes, followed by visible light irradiation from 0 to 90 minutes. Fixed conditions: 50 mg catalyst, 100 mL of 10 ppm dye solution, natural pH.

Binary solution of dyes

Finally, a binary solution of both the dyes was used to observe the simultaneous degradation of cationic and ionic dyes to highlights the materials efficacy due to its best results among others. A 10ppm binary solution of dyes (methyl orange and methyl green) in deionized water was prepared and irradiated under sunlight for regular intervals of time. As compared to the previous results for single dye solution the material also used showed significant degradation of dyes in mixture with for methyl orange. MO degradation was 81%, 78%, 79% in the presence of Cu-BTC@3A3NP, Cu-BTC@3A4HP, Cu-BTC@3A4H3MP in 90 minutes. Likewise, for methyl green 96%, 89% and 93% by using Cu-BTC@3A3NP, Cu-BTC@3A4HP, Cu-BTC@3A4H3MP as photocatalyst (**Figure 7 a-d & Figure S16)**. The implication of these results suggests that this material could be used to treat complex wastewater streams containing a mixture of different pollutants. From results it was concluded that our synthesized MOF showed excellent degradation efficiencies as compared to other reported materials **as given in Table 2**.

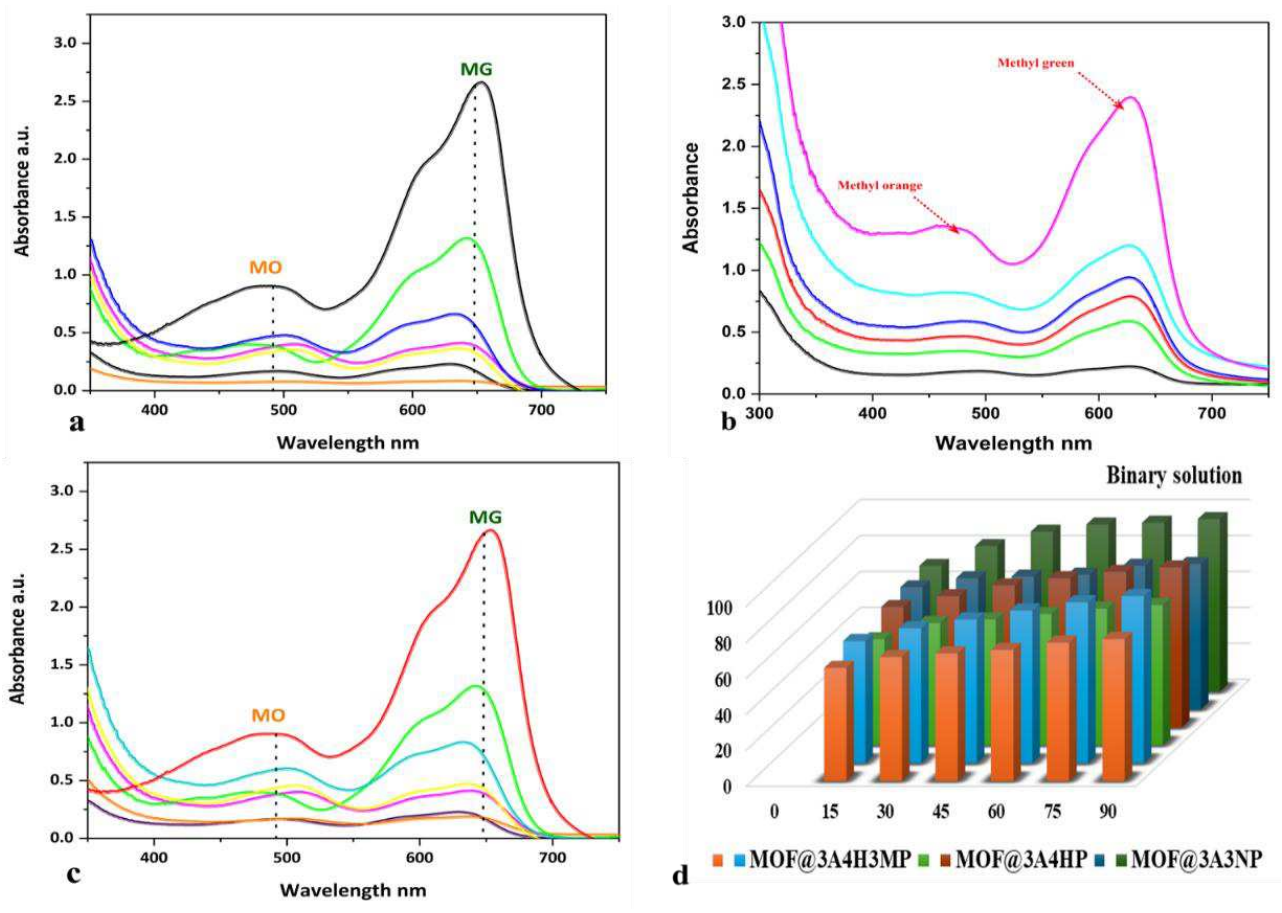


Figure 7. UV–Vis absorption spectra and degradation performance of MOF-based materials toward MO and MG dyes. (a) UV–Vis spectral changes of MO and MG in a binary dye mixture. (b) Comparative UV–Vis spectra of the binary MO–MG dye solution after treatment with different MOFs. (c) MO and MG during degradation using Cu-BTC@3A3NP. (d) Degradation efficiency (%) of MO and MG dyes in binary dye solutions using different modified MOFs, contact time (0–90 min), illustrating the superior performance of Cu-BTC@3A3NP.

Table 2. A comparison of the photocatalytic degradation efficiency of previously reported MOFs with Cu-BTC@3A3NP, Cu-BTC@3A4HP, Cu-BTC@3A4H3MP.

Photocatalyst	Photocatalyst dosage	Dye concentration	Time	%Degradation	Reference
Cu Co-ZIF	100mg	50mg/L(MO)	60min	99.4%	[63]
Cu Co-ZIF	50mg	40mg/L(MB)	100min	98%	[63]
HKUST-1	10mg	10mg/L(MB)	90min	53%	[64]
Cu (II)–[ABA–MA]	50mg	20mg/L(MB)	120min	93.6%	[65]
Cu-BTC	20mg	10mg/L(MB)	60min	95.2%	[6]
Co-MOF-74	30mg	10mg/L(RhB)	180min	95.2%	[66]
Amino-MOF-1	50mg	20mg//L(MB)	120min	92.5%	[67]
Cu-BTC@3A3NP	50mg	10mg/L(MO)	70min	88%	This study
Cu-BTC@3A3NP	50mg	10mg/L(MG)	70min	96%	This study
Cu-BTC@3A4HP	50mg	10mg/L (MO)	70min	81%	This study
Cu-BTC@3A4HP	50mg	10mg/L (MG)	70min	94%	This study
Cu-BTC@3A4H3MP	50mg	10mg/L (MO)	70min	83%	This study
Cu=BTC@3A4H3MP	50mg	10mg/L (MG)	70min	95%	This study

Proposed Mechanism

The exceptional photocatalytic performance of amino acid-modified Cu-BTC MOF in degrading methyl green and methyl orange has been previously discussed. To understand this phenomenon, it's crucial to elucidate the underlying mechanism. The photocatalytic process is initiated by the generation of electron-hole pairs between the valence and conduction bands, leading to the degradation of dyes. To comprehend this process, determining the positions of the valence and conduction bands of the semiconductor is essential. This knowledge will shed light on the electronic transitions involved in the photocatalytic reaction, allowing for a deeper understanding of the mechanism[68].

The valence band (VB) and conduction band (CB) positions of the amino acid-modified Cu-BTC MOF can be estimated using the band gap energy by following these equations:

$$E_{CB} = X - E_e - 0.5E_g \quad (4)$$

$$E_{VB} = X - E_{CB} + E_g \quad (5)$$

$$X = [\chi(A)^a + \chi(B)^b + \chi(C)^c]^{\frac{1}{a+b+c}} \quad (6)$$

β-amino acid modified Cu-BTC MOF has a valence band (E_{VB}) value of 1.85eV and a conduction band (E_{CB}) value of -0.75 eV for Cu-BTC@3A3NP, valence band (E_{VB}) value of 1.75eV. The conduction band (E_{CB}) value of -0.25 eV, for Cu-BTC@3A4HP and valence

band (E_{VB}) value of 2.05eV and a conduction band (E_{CB}) value of -0.525 eV, for Cu-BTC@3A4H3MP. Thus, the materials are assumed to be p-type semiconductors, with a Fermi level located near the valence band edge, indicating hole transfers. The positive valence band value and negative conduction band value facilitate oxidation and reduction reactions, respectively, making this material suitable for photocatalytic applications [69, 70]. Reactive oxygen species (ROS) induce the photocatalytic degradation of azo dyes, cleaving the azo link and resulting in colour loss (**Figure S16**). Amino acid-modified MOFs improve this process by increasing light absorption, charge carrier separation, ROS production, and stability. ROS destroy the azo link in dyes such as MO and methyl green, breaking conjugation and causing colour loss, consistent with the decrease in absorption according to UV-vis analysis, as colour changes specifically from orange to colourless and green to colourless (**Figure 8**). Combining amino acid-modified MOFs and ROS results in effective azo dye degradation, making it a viable alternative for wastewater treatment and environmental remediation [71].

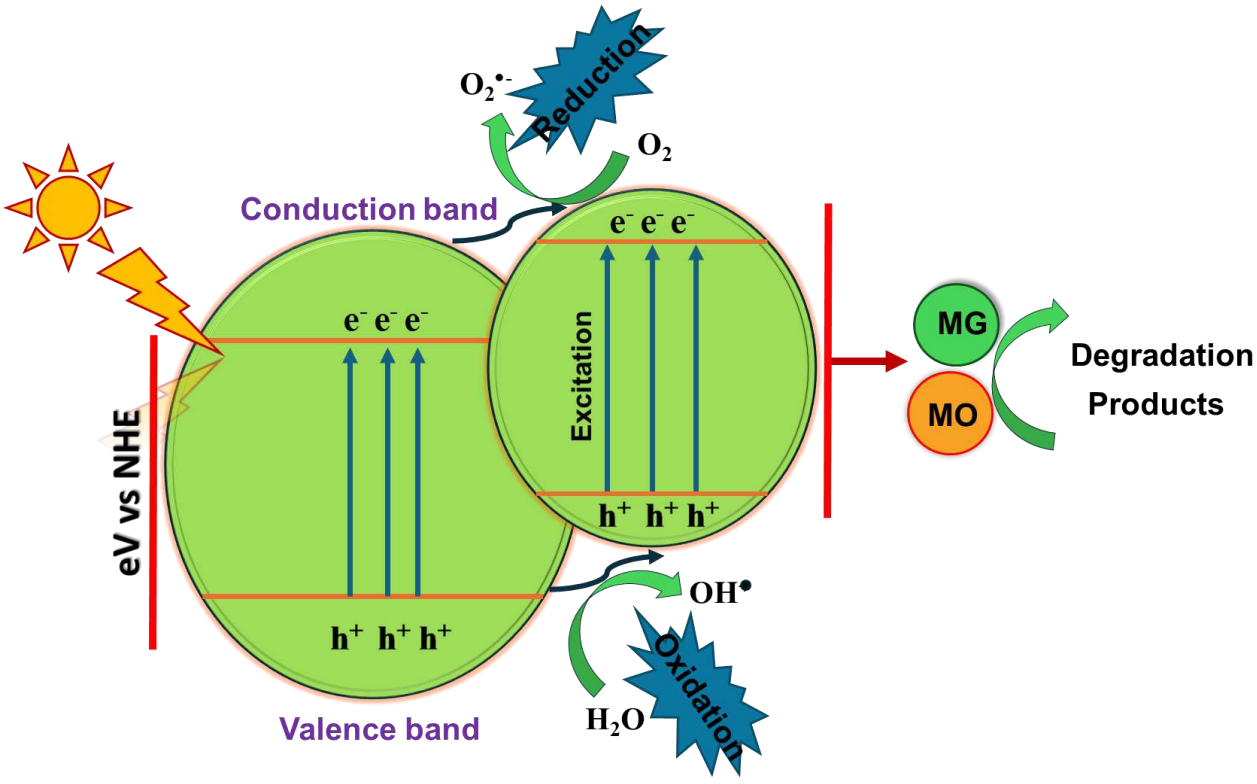


Figure 8. Proposed mechanism of photocatalytic dye degradation by β-amino acid modified metal organic frameworks.

$$(\text{Amino/Cu BTC}) + \text{hv} \rightarrow (\text{Amino/Cu BTC})(e^- + h^+) \quad (7)$$

$$(\text{Amino/Cu BTC})(e^-) + O_2 + \rightarrow + O_2^{\bullet -} \quad (8)$$

$$(\text{Amino/Cu BTC})(h^+) + H_2O + e^- \rightarrow + OH^{\bullet} \quad (9)$$

$$O_2^{\bullet -} + \text{MO/MG} \rightarrow \text{Harmless degradation product} + H_2O \quad (10)$$

$$OH^{\bullet} + \text{MO/MG} \rightarrow \text{Harmless degradation product} + H_2O \quad (11)$$

It is important to note that while the observed reduction in the optical band gap and the enhanced photocatalytic activity strongly suggest improved visible-light harvesting and more efficient charge separation, direct experimental validation of charge carrier dynamics (e.g., via photoluminescence or electrochemical impedance spectroscopy) and specific surface area changes (BET analysis) were beyond the scope of the current study due to instrumental constraints. These mechanistic inferences are strongly supported by established literature on functionalized MOFs. Comprehensive structure–property–activity relationship studies utilizing these advanced techniques are currently underway and will be the focus of our immediate future research.

Conclusion

In conclusion, this study successfully demonstrates the synthesis, structural retention, and enhanced visible-light photocatalytic activity of novel β-amino-functionalized Cu-BTC composites. PXRD, FTIR, and SEM analyses confirmed the successful post-synthetic modification and morphological changes, while UV-Vis spectroscopy revealed a significant reduction in the optical band gap. These modifications led to superior photocatalytic performance, achieving up to 99% degradation of methyl green and methyl orange under visible light.

While this work provides compelling evidence for the efficacy of these functionalized MOFs, we acknowledge that a comprehensive elucidation of the structure–property–activity relationships requires further advanced characterization. Due to current instrumental limitations, direct measurements of specific surface area (BET), charge carrier dynamics (e.g., photoluminescence or electrochemical impedance spectroscopy), and long-term hydrothermal stability were not included in this study. The claims regarding enhanced charge separation and

surface properties are currently inferred from the observed optical and photocatalytic data, consistent with literature on similar systems. Addressing these aspects through detailed mechanistic and advanced physicochemical studies is the primary objective of our ongoing and future research. Ultimately, the findings presented here highlight the promising potential of β-amino-functionalized Cu-BTC as a robust photocatalyst for environmental remediation. The mechanistic inferences regarding charge separation are currently supported by the observed optical/photocatalytic data and established literature on similar systems. Comprehensive structure–property–activity relationship studies utilizing these advanced techniques are the primary objective of our ongoing and future research.

Author contributions

The specification of individual contribution of each author is as follows:

a. **Nagina Naveed Riaz**: Conceptualization, Data correction, Formal analysis, Investigation, Software, Project Administration, Resources, Validation, Visualization, Writing original draft, Writing-review & editing.
b. **Ayesha Faraz**: Data correction, Formal analysis, Investigation, Resources, Software, Visualization, Writing original draft, Writing-review & editing.
c. **Khalil Ahmad**: Data correction, Software, Validation, Visualization, Writing-review & editing.
d. **Ejaz Hussain**: Data correction, Software, Validation, Visualization,
e. **Muhammad Fiaz**: Data correction, Software, Validation, Visualization.
f. **Muhammad Mahboob Ahmad**: Data correction, Formal analysis, Investigation, Software, Resources, Validation, Visualization, Writing original draft, Writing-review & editing.
g. **Muhammad Kashif and Ahmad Hosseini Bandegharaei**: Supervision, Data correction, Formal analysis, Investigation, Software, Resources, Validation, Writing-review & editing

Conflicts of interest

There are no conflicts of interest to declare.

Data availability

The data supporting this article have been included as part of the Supplementary Information.

Funding Declaration

There was no Funding received during this manuscript.

Acknowledgements

The authors are very thankful to the Department of Chemistry, University of Education, Vehari Campus, Lahore, Pakistan for providing research facilities. The Department of Chemistry, GC University, Faisalabad Pakistan is also acknowledged for spectroscopic analysis.

References:

1. Padmanabhan, N. T., Gayathri, K., Thomas, R. M., & John, H, Energy & Environmental Sustainability, 2025, **1(3)**, 100042.
2. Zhong, R., Lyu, H., Su, X., Yan, X., Teng, Y., Dong, W, Shen, X, Water Research, 2025, 124495.
3. Ma, Q., Qian, Y., Su, W., Shi, L., Wang, E., Yu, A, Lu, Y, Ecotoxicology and Environmental Safety, 2025, **303**, 118841.
4. Lu, J. Y., Bu, Z. Q., Lei, Y. Q., Wang, D., He, B., Wang, J, Huang, W. T, Journal of Molecular Liquids, 2024, **409**, 125503.
5. S. Rojas and P. Horcajada, *Chemical reviews*, 2020, **120**, 8378-8415.
6. A. Singh, A. K. Singh, J. Liu and A. Kumar, *Catalysis Science & Technology*, 2021, **11**, 3946-3989.
7. M. N. Nimbalkar and B. R. Bhat, *Journal of Environmental Chemical Engineering*, 2021, **9**, 106216.
8. Yang, X., Luo, S., Zhou, J., Sun, P., Guo, Y., Zhao, J, Gao, B, Industrial Crops and Products, 2025, **235**, 121777.
9. T. C. Maponya, M. J. Hato, E. Makhado, K. Makgopa, M. Khanuja and K. D. Modibane, in *Metal, Metal-Oxides and Metal-Organic Frameworks for Environmental Remediation*, Springer, 2021, pp. 261-285.
10. Guo, L., Chen, W., Wang, C., & Dong, B, International Journal of Electrochemical Science, 2023, **18(1)**, 26-32.
11. A. Dutta, Y. Pan, J.-Q. Liu and A. Kumar, *Coordination Chemistry Reviews*, 2021, **445**, 214074.
12. M. Kasula, T. Le, A. Thomsen and M. R. Esfahani, *Chemical Engineering Journal*, 2022, **439**, 135542.
13. J. Liu, Y. Zhou, Z. Xie, Y. Li, Y. Liu, J. Sun, Y. Ma, O. Terasaki and L. Chen, *Angewandte Chemie International Edition*, 2020, **59**, 1081-1086.
14. W. Liu, X. Shen, Y. Han, Z. Liu, W. Dai, A. Dutta, A. Kumar and J. Liu, *Chemosphere*, 2019, **215**, 524-531.
15. S. Xie, Q. Liu, F. Zhu, M. Chen, L. Wang, Y. Xiong, Y. Zhu, Y. Zheng and X. Chen, *Journal of Materials Chemistry C*, 2020, **8**, 10408-10415.
16. A. C. Tella, J. T. Bamgbose, V. O. Adimula, M. Omotoso, S. E. Elaigwu, V. T. Olayemi and O. A. Odunola, *SN Applied Sciences*, 2021, **3**, 1-15.

17. S. Zhao, S. Li, Z. Zhao, Y. Su, Y. Long, Z. Zheng, D. Cui, Y. Liu, C. Wang and X. Zhang, *Environmental Science and Pollution Research*, 2020, **27**, 39186-39197.
18. X. Zhang, J. Wang, X.-X. Dong and Y.-K. Lv, *Chemosphere*, 2020, **242**, 125144.
19. B. Liu, K. Vikrant, K.-H. Kim, V. Kumar and S. K. Kailasa, *Environmental Science: Nano*, 2020, **7**, 1319-1347.
20. M. N. Ahamad, M. S. Khan, M. Shahid and M. Ahmad, *Dalton Transactions*, 2020, **49**, 14690-14705.
21. P. Goyal, D. Menon, P. Jain, P. Prakash and S. K. Misra, *Separation and Purification Technology*, 2023, **318**, 123941.
22. D. Zou and D. Liu, *Materials Today Chemistry*, 2019, **12**, 139-165.
23. M. Ding and H.-L. Jiang, *CCS Chemistry*, 2021, **3**, 2740-2748.
24. S. Feng, M. Bu, J. Pang, W. Fan, L. Fan, H. Zhao, G. Yang, H. Guo, G. Kong and H. Sun, *Journal of membrane science*, 2020, **593**, 117404.
25. Y. Hu, Z. Fang, X. Wan, X. Ma, S. Wang, S. Fan, M. Dong, Z. Ye and X. Peng, *Chemical Engineering Journal*, 2022, **430**, 133086.
26. P. Arul, N. Gowthaman, S. A. John and M. Tominaga, *Electrochimica Acta*, 2020, **354**, 136673.
27. Y.-J. Tong, L.-D. Yu, J. Zheng, G. Liu, Y. Ye, S. Huang, G. Chen, H. Yang, C. Wen and S. Wei, *Analytical chemistry*, 2020, **92**, 15550-15557.
28. B. Szczęśniak, J. Phuriragpitikhon, J. Choma and M. Jaroniec, *Journal of Colloid and Interface Science*, 2020, **577**, 163-172.
29. X. Wang, X. Zhang, K. Zhang, X. Wang, Y. Wang, W. Fan and F. Dai, *Inorganic Chemistry Frontiers*, 2019, **6**, 1152-1157.
30. G. Gizer, M. Sahiner, Y. Yildirim, S. Demirci, M. Can and N. Sahiner, *Current Research in Green and Sustainable Chemistry*, 2021, **4**, 100110.
31. Y. Zhang, Z. Li, F. Gao, Z. Ma, W. Li, X. Gao and G. Fan, *Journal of Solid State Chemistry*, 2022, **316**, 123551.
32. S. Guo, J. Zhu and S. L. J. A. C. Buchwald, 2020, **132**, 21027-21031.
33. Qi, Z., An, Z., Huang, B., Wu, M., Wu, Q, Jiang, D, Organic & Biomolecular Chemistry, 2023, **21(31)**, 6419-6423.
34. V. Subramaniyam, P. V. Ravi and M. Pichumani, *Journal of Molecular Structure*, 2022, **1251**, 131931.
35. P. Mei, Y. Zhang and X. Feng, *Acta Chimica Sinica*, 2020, **78**, 1041.
36. E. Amdeha and R. S. Mohamed, *Environmental Technology*, 2021, **42**, 842-859.
37. Y. Fang, Z. Yang, H. Li and X. Liu, *Environmental Science and Pollution Research*, 2020, **27**, 4703-4724.
38. L. Liu, X.-L. Chen, M. Cai, R.-K. Yan, H.-L. Cui, H. Yang and J.-J. Wang, *Spectrochimica Acta Part A: Molecular and Biomolecular Spectroscopy*, 2023, **289**, 122228.
39. F. Guo, M. Yang, R.-X. Li, Z.-Z. He, Y. Wang and W.-Y. Sun, *ACS Catalysis*, 2022, **12**, 9486-9493.
40. C. Yan, X. Dong, Y. Wang, N. Zheng, H. Ma and X. Zhang, *Journal of Water Process Engineering*, 2023, **55**, 104224.
41. X. Li, Y. Wang and Q. Guo, *Heliyon*, 2022, **8**.

42. M. M. Ahmed, N. N. Riaz, M. Kashif, M. Ashfaq, M. N. Arshad and M. Sajid, *Journal of the Brazilian Chemical Society*, 2021, **32**, 1082-1099.
43. L. Rasuli, M. H. Dehghani, M. Alimohammadi, K. Yaghmaeian, N. Rastkari and M. J. J. o. M. L. Salari, Journal of Molecular Liquids, 2021, **339**, 116801.
44. R. Rani, A. Deep, B. Mizaikoff and S. J. V. Singh, Vacuum, 2019, **164**, 449-457.
45. T. Noor, M. Ammad, N. Zaman, N. Iqbal, L. Yaqoob and H. Nasir, *Catalysis Letters*, 2019, **149**, 3312-3327.
46. Y. Liu, P. Ghimire and M. Jaroniec, *Journal of colloid and interface science*, 2019, **535**, 122-132.
47. L. Qiao, A. Zhu, Y. Liu, Y. Bian, R. Dong, D. Zhong, H. Wu and J. Pan, *Journal of materials science*, 2018, **53**, 7755-7766.
48. N. T. Phuong, C. Buess-Herman, N. T. Thom, P. T. Nam, T. D. Lam and D. T. M. Thanh, *Green Processing and Synthesis*, 2016, **5**, 537-547.
49. D. N. Lee, Y. R. Kim, S. Yang, N. M. Tran, B. J. Park, S. J. Lee, Y. Kim, H. Yoo, S.-J. Kim and J. H. Shin, *International Journal of Molecular Sciences*, 2022, **23**, 9098.
50. S. Hao and Y. Liu, *Journal of Materials Science*, 2022, **57**, 1689-1702.
51. J. De Meutter and E. Goormaghtigh, *European Biophysics Journal*, 2021, **50**, 641-651.
52. P. Kavaliauskas, B. Grybaitė, B. Sapijanskaitė-Banevič, R. Vaickelionienė, V. Petraitis, R. Petraitienė, E. Naing, A. Garcia, R. Grigalevičiūtė and V. Mickevičius, *Antibiotics*, 2024, **13**, 193.
53. S. A. Siddiqui, A. Prado-Roller and H. Shiozawa, *Materials Advances*, 2022, **3**, 224-231.
54. K. Peikert, F. Hoffmann and M. Fröba, *Chemical communications*, 2012, **48**, 11196-11198.
55. B. Venu, V. Shirisha, B. Vishali, G. Naresh, R. Kishore, I. Sreedhar and A. Venugopal, *New Journal of Chemistry*, 2020, **44**, 5972-5979.
56. M. Yan, Y. Zhang, G. Zhu, X. Kong, T. Cang, D. Wang, H. Wibowo and E. Kanchanatip, *Environmental Science and Pollution Research*, 2024, **31**, 35979-35991.
57. E. Haque, J. E. Lee, I. T. Jang, Y. K. Hwang, J.-S. Chang, J. Jegal and S. H. Jhung, *Journal of hazardous materials*, 2010, **181**, 535-542.
58. M. Adeel, M. Saeed, I. Khan, M. Muneer and N. Akram, *ACS omega*, 2021, **6**, 1426-1435.
59. Z. Li, D. Ren, Z. Wang, S. Jiang, S. Zhang, X. Zhang and W. Chen, *Water Science and Technology*, 2022, **86**, 80-94.
60. E. A. Kozlova, V. N. Panchenko, Z. Hasan, N. A. Khan, M. N. Timofeeva and S. H. Jhung, *Catalysis Today*, 2016, **266**, 136-143.
61. S. Sadeghian, H. Pourfakhar, M. Baghdadi and B. Aminzadeh, *Chemosphere*, 2021, **268**, 129365.
62. M. Saeed, M. Muneer, A. u. Haq and N. Akram, *Environmental Science and Pollution Research*, 2022, **29**, 293-311.
63. T. H. Luong, T. H. Nguyen, B. V. Nguyen, N. K. Nguyen, T. Q. Nguyen and G. H. Dang, *Green Processing and Synthesis*, 2022, **11**, 71-83.
64. J. Zhang, C. Su, X. Xie, P. Liu and M. E. Huq, *RSC advances*, 2020, **10**, 37028-37034.

65. M. Arif, U. Fatima, A. Rauf, Z. H. Farooqi, M. Javed, M. Faizan and S. Zaman, *Catalysts*, 2023, **13**, 231.
66. M.-A. Gatou, I.-A. Vagena, N. Lagopati, N. Pippa, M. Gazouli and E. A. Pavlatou, *Nanomaterials*, 2023, **13**, 2224.
67. W. Fan, X. Wang, B. Xu, Y. Wang, D. Liu, M. Zhang, Y. Shang, F. Dai, L. Zhang and D. Sun, *Journal of Materials Chemistry A*, 2018, **6**, 24486-24495.
68. A. Haleem, M. Ullah, A. Shah, M. Farooq, T. Saeed, I. Ullah and H. Li, *Water*, 2024, **16**, 1588.
69. X. Guo, L. Liu, Y. Xiao, Y. Qi, C. Duan and F. Zhang, *Coordination Chemistry Reviews*, 2021, **435**, 213785.
70. J. Li, T. Musho, J. Bright and N. Wu, *Journal of The Electrochemical Society*, 2019, **166**, H3029-H3034.
71. Q. Wang, Q. Xu, J. Zhang, L. Fang, K. Xia and D. Sun, *Fine Chemical Engineering*, 2024, 36-48.

Supplementary Files

This is a list of supplementary files associated with this preprint. Click to download.

- SIsubmitted.docx